Characterization of Arsenic in dried baby shrimp (Acetes sp.) using synchrotron-based X-Ray Spectrometry and LC coupled to ICP-MS/MS

Journal:	*Journal of Analytical Atomic Spectrometry*
Manuscript ID	JA-ART-04-2018-000094.R2
Article Type:	Paper
Date Submitted by the Author:	17-Jul-2018
Complete List of Authors:	Guimarães, Diana; Centro de Física Atomica (CFA/FCUL), Departamento de Física, Faculdade de Ciências e Tecnologia, FCT, Universidade Nova de Lisboa, Physics Department Roberts, Austin; New York State Dept of Health, Lab of Inorganic and Nuclear Chem; University at Albany, Environmental Health Sciences Tehrani, Mina; New York State Dept of Health, Lab of Inorganic and Nuclear Chem; University at Albany, Environmental Health Sciences Huang, Rong; Cornell University High Energy Synchrotron Source, Smieska, Louisa; Cornell University High Energy Synchrotron Source Woll, Arthur; Cornell University High Energy Synchrotron Source Lin, Shao; University at Albany, Environmental Health Sciences Parsons, Patrick; New York State Dept of Health, Lab of Inorganic and Nuclear Chem; University at Albany, Environmental Health Sciences

Characterization of Arsenic in dried baby shrimp (*Acetes sp.*) using synchrotron-based X-Ray Spectrometry and LC coupled to ICP-MS/MS

Diana Guimarães[†1,2], Austin A. Roberts[1,2]; Mina W. Tehrani[1,2]; Rong Huang[3], Louisa Smieska[3], Arthur R. Woll[3], Shao Lin[2] and Patrick J. Parsons*[1,2]

[1] Laboratory of Inorganic and Nuclear Chemistry, Wadsworth Center, New York State Department of Health, P.O. Box 509, Albany, NY 12201-0509, USA
[2] Department of Environmental Health Sciences, School of Public Health, The University at Albany, P.O. Box 509, Albany, NY 12201-0509, USA
[3] Cornell High Energy Synchrotron Source, Cornell University, Ithaca, USA

E-mail: patrick.parsons@health.ny.gov; Fax: +1 518-473-2895; Tel: +1 518-474-7161

* author for correspondence

[†]current address: INESC TEC, Campus da FEUP, Rua Dr. Roberto Friãs, 4200 - 465 Porto, Portugal

Abstract

The arsenic content of dried baby shrimp (*Acetes sp.*) was investigated as part of an independent field study of human exposure to toxic metals/metalloids among the ethnic Chinese community located in Upstate New York. The dried baby shrimp were analyzed in a home environment using a portable X-ray Fluorescence (XRF) instrument based on monochromatic excitation. Study participants had obtained their dried baby shrimp either from a local Chinese market or prepared them at home. The shrimp are typically between 10-20 mm in size and are consumed whole, without separating the tail from the head. Elevated levels of As were detected using portable XRF, ranging between 5-30 µg/g. Shrimp samples were taken to the Cornell High Energy Synchrotron Source (CHESS) for Synchrotron Radiation µXRF (SR-µXRF) elemental mapping using a 384-pixel Maia detector system. The Maia detector provided high resolution trace element images for As, Ca, and Br, (among others) and showed localized accumulation of As within the shrimp's cephalothorax (head), and various abdominal segments. As quantification by SR-µXRF was performed using a Lobster hepatopancreas reference material pellet (NRC-CNRC TORT-2), with results in good agreement with both portable XRF and ICP-MS. Additional As characterization using µX-ray Absorption Near Edge Spectroscopy (µXANES) with the Maia XRF detector at CHESS identified arsenobetaine and/or arsenocholine as the possible As species present. Further arsenic speciation analysis by LC-ICP-MS/MS confirmed that the majority of As (>95%) is present as the largely non-toxic arsenobetaine species with trace amounts of arsenocholine, methylated As and inorganic As species detected.

Keywords: As, Shrimp, seafood, portable XRF, SR-µXRF, elemental mapping, Maia detector, µXANES Trace element distribution, LC-ICP-MS/MS

Introduction

In the last two decades there has been a remarkable growth in aquaculture production and trade. Imports and exports of seafood have increased to meet the demands of high-value species like prawns, shrimp and salmon, but also other low-value species as tilapia and cat-fish.[1] Shrimp farming is one of the most profitable aquaculture industries and a consequence of overfishing wild-caught seafood.[2] In China, baby shrimp (*Acetes sp.*) are mostly consumed whole after being drying and salted. The process derives from ancient China, when there was a need to store food long-term. [3] Shrimp are traditionally salted and either sun-dried or dried using commercial dryers. The drying process enhances the taste of the shrimp, which may be added to foods such as vegetables, soups and stuffing, and used as a flavoring agent and as a protein source. [3, 4]

Diets rich in seafood raise concerns about overexposure to toxic contaminants, including heavy metals and some metalloids. [5] Arsenic bioaccumulates in certain seafoods due to natural and anthropogenic sources. [6, 7] However, the toxicity of As depends on its chemical form which can pose different risks depending on the particular As species. Inorganic As species such as As(III) (arsenite) and As(V) (arsenate) are considered much more toxic than organoarsenic species such as arsenobetaine. [8] Inorganic As is found in water, while marine organisms contain mainly organoarsenic compounds that are biosynthesized from the inorganic. [9]

While some studies report the total elemental content of bulk seafood, it is possible to use elemental imaging techniques to obtain a more detailed picture on the spatial distribution of some elements. However, quantifying the elemental content can be challenging due to issues such as matrix effects and calibration difficulties. [10, 11] Current elemental imaging techniques include Laser Ablation Inductively Coupled Plasma Mass Spectrometry (LA-ICP-MS) and X-ray based techniques such as Electron Microprobe Analysis (EMPA), Proton Induced X-ray Emission (PIXE) and X-ray Fluorescence (XRF).[12-14] X-ray techniques based on energy dispersive spectrometry (EDS) that use a scanning electron microscope (SEM) or scanning transmission electron microscope (STEM) can have micron- and even nano-scale mapping capabilities but are often semi-quantitative with poorer detection limits compared to

XRF.[13, 15] LA-ICP-MS can achieve detection limits in the ng/g range although quantitation is often challenging, especially for biological matrices, and the laser ablation process results in some destruction of the sample surface. [16] Both PIXE and XRF can achieve µg/g detection limits at the micron scale, are non-destructive and reasonably quantitative depending on the approach used. However, PIXE has a shorter analytical depth and needs longer acquisition times. [13] Elemental imaging at the micron level using Synchrotron Radiation µXRF (SR-µXRF) continues to gain more visibility in environmental, biological and food studies, among others. [12] Advances in the focusing optics have produced sub-micrometer probes to enhance spatial resolution for imaging.[13, 17] Additional improvements include a new generation of XRF detectors and digital pulse processors that, together, permit count rates that are 10- to 100 times higher than those previously available,[18, 19] enabling shorter acquisition times to scan across larger sample areas at rapid speeds.

Several studies have reported elemental imaging of food and biological samples [12, 16, 20-23] but few have included shrimp species. Two previous studies reported elemental mapping of fossilized shrimp from the Cretaceous Period, [24, 25] and another focused on the microstructure of the Mantis shrimp saddle. [26] In another study of food samples commonly consumed in Bangladesh, prawns and other freshwater fish were analyzed for total (bulk) As content (along with other elements) using PIXE and radioisotope-excited XRF. [27] Here we report on the characterization of As found in samples of dried baby shrimp delicacy, analyzed during the course of a field-based research study of human exposure to toxic metals/metalloids in cultural food products. The shrimp delicacy was analyzed for elemental content, using a portable XRF analyzer equipped with monochromatic excitation based on doubly-curved crystal optics. The novel aspects of this new portable XRF technology have been described previously. [28] Additional investigations of the dried baby shrimp were carried out at the Cornell University High Energy Synchrotron Source (CHESS), using SR-µXRF and Micro X-ray Absorption Near Edge Spectroscopy (µXANES) with a multi-array Si PIN detector (Maia). This 384-element X-ray detector was used to produce high-resolution elemental images of the dried baby shrimp from XRF spectra, along with regional µXANES analyses that provided additional characterization on As. The As content of these shrimp samples were characterized yet further using liquid chromatography (LC-) coupled to ICP-MS, which provided a more selective approach to As speciation compared to µXANES.

Experimental

Reference materials, arsenic standards, and study samples

Certified Reference Materials (CRM) were obtained from various sources to validate XRF elemental data and to serve as quality control (QC) materials. The latter task was accomplished by analyzing IAEA-413 Major, Minor, and Trace Elements in Algae (International Atomic Energy Agency, Vienna, Austria) using the XRF portable instrument at the beginning and end of each home visit. In addition, a boric acid blank (99.9995% H_3BO_3 — Alfa AESAR, Ward Hill, MA) was analyzed in the field to check for contamination. XRF measurement accuracy for the portable XRF and SR-μXRF systems was assessed with (a) NIST (National Institute of Standards and Technology, Gaithersburg, MD) Standard Reference Material (SRM) 2976 Mussel Tissue (Trace elements and methylmercury) and (b) NRC TORT-2 Lobster Hepatopancreas Reference Material for Trace Metals (National Research Council, Ottawa, Canada). An additional reference material NRC DORM-2 Dogfish Muscle for Trace Metals, was also used for μXANES. While the certificate of analysis for DORM-2 had previously expired, the AsB content was checked using LC-ICP-MS along with other CRMs. For As speciation performed by LC-ICP-MS, IRMM BCR-627 – Forms of arsenic in tuna fish tissue (Institute for Reference Materials and Measurements, Geel, Belgium) and NRC DORM-4 Fish protein (NRC, Ottawa, Canada) were analyzed in addition to NRC DORM-2. Additional reference materials were used to validate total As measurements: NRC TORT 3 - Lobster Hepatopancreas (NRC, Ontario, Canada) and New York State Caprine Liver Reference Materials, G99-3 and G99-14 (New York State Dept. of Health; Wadsworth Center, Albany, NY). All CRMs and RMs were stored at 4 °C.

Several foils (Micromatter, Vancouver, BC) were used as calibration standards for the SR-μXRF and μXANES studies: Pt (18.0 μg/cm^2), Cu (15.9 μg/cm^2), Ti (21.2 μg/cm^2) and Au (19.2 μg/cm^2).

Different chemical compounds containing arsenic as powdered samples were used for μXANES speciation: dimethylarsinic acid (DMA, purity 99.5%) and disodium methyl arsonate hexahydrate (DSMA, purity 97.4%), a precursor of MMA, were obtained from Chem Service, Inc (West Chester, Pennsylvania, USA); arsenobetaine (AsB, purity ≥ 95.0%); As(V) oxide hydrate (purity 97%) and As(III) oxide (purity >

99.5%) were obtained from Sigma-Aldrich (St. Louis, Missouri, USA); and arsenocholine bromide (AC, purity 95%) was purchased from Toronto Research Chemicals Canada (TRC-Canada, Ontario, Canada). For As speciation by LC-ICP-MS, calibration standards were prepared from 10 mg L^{-1} (as As) stock solutions, checked for impurities, and used to identify and quantitate up to six As species.

Dried baby shrimp (*Acetes sp.*)

During the course of a home study involving the Chinese community of upstate New York, three samples of different dried baby shrimp products were analyzed for elemental content using a portable XRF device, and samples brought back to the laboratory for further analyses. One of the samples (sample A) was prepared at home by the study subject while the other two (samples B and C) were commercial products purchased from local Chinese markets: sample B was labelled “Rely Dried Shrimp” and sample C was labelled “Wei Chuan Dried Shrimp (Baby)”. These products range in size from 10 - 20 mm and are typically consumed whole without separating the tail from the shrimp head.

Instrumentation and Methods

Portable XRF analyzer

For field measurements, a portable XRF analyzer HD Mobile® (X-ray Optical Systems, East Greenbush, NY) was used. The portable XRF uses a Mo-anode X-ray tube operated at 50 kV, and 0.1 mA current. The analyzer uses a doubly curved crystal (DCC) optic to focus the excitation X-ray beam into a 1-mm spot size. The proprietary DCC optics provide monochromatic excitation at three energies: 6.4 keV, 17.4 keV and 34 keV. The monochromatic beam excites the sample at each of the three energies during analysis leading to a background reduction and sensitivity enhancement. [29] For the detection of the emitted X-ray fluorescence, a silicon drift detector (SDD) was used.

The portable XRF analyzer was used as an integrated system within its case/stand rather than in hand-held mode to improve performance. We used the “plastic” measurement mode with a measurement time of 3 minutes for quantitative results, as this had been previously validated for these types of samples. [28]

As mentioned above, IAEA Algae-413 reference material (RM) was analyzed as a QC sample along with a boric acid blank at every run. Data processing was performed using the XOS "Solver", a proprietary program based on fundamental parameters method that is integrated into the portable XRF. [30]

For the analysis of RMs and shrimp specimens, a portion of the sample was placed inside a 10-mL polyethylene XRF cup (Premier Lab Supply, Port St. Lucie, FL) containing a 4-μm thick polypropylene window. The XRF cups were filled such that the sample depth was at least 1 cm, to ensure infinite path thickness. In practical terms, depending on the measurement location, multiple shrimp can be interrogated by the X-ray beam at the same time. Under field conditions, only one replicate was analyzed.

SR-μXRF and μXANES

All synchrotron measurements were performed at the F3 beam line at CHESS, including μXRF imaging and μXANES. The source of the intense synchrotron radiation is a 5.3 GeV positron beam that passes through a bending magnet inside the Cornell Electron Storage Ring (CESR), with a circumference of 768 m. A monochromator is used to select the beam energy, arriving from the white beam radiation source, before being delivered to experimental hutch. For the pilot μXRF maps, a double-crystal Si (111) monochromator was used, while for the main study we used a Si (220) monochromator. The two monochromators have different energy bandwidths, and thus different flux densities. Selecting the Si (220) monochromator provides a narrower bandwidth and a better energy resolution ($\Delta E/E \sim 10^{-4}$) but a lower X-ray flux density.

To focus the X-ray beam without losing flux, a unique single bounce 115-mm long monocapillary (PEb605) was used. [31, 32] This monocapillary produces a 20-μm spot size 55 mm from the capillary tip. An X-ray beam stop was used upstream of the capillary to block all X-rays that would otherwise pass through the center opening of capillary without being reflected. Compared to an unfocused beam, the capillary increases flux density at the focal center by a factor of 450. The total flux employed for the measurements described here was approximately 5×10^{8} photons/second in the focal spot. Monochromator and capillary alignment was monitored using a set of three ion chambers located: (i) after the beam first enters the hutch; (ii) just after a beam cleaning slit and before the beam enters the capillary, and (iii) downstream of sample.

To perform μXRF and μXANES measurements, each shrimp sample and reference material was mounted between two layers of 0.0025'' Kapton® polyimide tape (McMaster-Carr, Elmhurst, Illinois, USA) as shown in Fig. 1a. A sample of each As standard (as a powder) was transferred inside a Teflon washer (inner diameter of 3 mm, 0.8 mm thickness) placed on Kapton tape, and then sealed using another piece of Kapton tape as shown in Fig. 1b. μXRF spectra were obtained at 20 keV (for the pilot data) and at 16.15 keV (for the main study), with a 384-element Maia detector[19] operated in backscatter geometry,[19, 33, 34] with a sample-to-detector distance of 2-mm. The Maia detector is equipped with an array of 384 individual Si PIN diodes, that allows real-time processing/spectral deconvolution and imaging at photon rates exceeding 10^7 counts/s and 50 μs/pixel,[19] compared with count rates of 10^5-10^6 c/s and dwell times exceeding 50 μs for conventional single-element or quad-element detectors. The Maia detector dramatically enhances sensitivity for trace elements affording high definition imaging over larger areas in a much shorter time than was previously possible. Using this arrangement, SR-μXRF elemental images were obtained by continuously scanning the samples horizontally with a step size of 20 μm and dwell time of 50 ms per step. In a follow-up study, As μXANES 2D maps were also obtained in fluorescence mode by repeatedly scanning a region of interest, sequentially increasing the incident energy for each μXRF map to step through the As edge. Specifically, the incident energy was adjusted from 11.850 keV to 11.900 keV in 1 eV increments. These μXRF spectra for the μXANES maps, were acquired with a dwell time of 5 ms for calibration foils, As standards and a reference material pellet, and a dwell time of 40 ms for the shrimp samples.

After the μXRF spectra were collected, they were analyzed using GeoPIXE™ v7.2 [33, 35, 36] software to yield elemental concentration images and μXANES maps. GeoPIXE™ uses the Dynamic Analysis method that subtracts the background and resolves peak overlaps in order to build elemental maps. Quantification is achieved using the fundamental parameters method, [30] that predicts the mass fraction based on the intensity of the fluoresced X-rays, taking into account various parameters such as X-ray ionization cross-sections, self-absorption in the sample and in air, sample-detector distances, fluorescence yields, and detector efficiency. The latter was obtained using several reference foils of known mass fraction to calibrate the incident flux. In order to calculate the fluorescence yields accurately, used as an input parameter of GeoPIXE™, both sample composition and the area density (g/cm^2) should

be known. First, because shrimp and biological reference materials are not easily described with a unique chemical formula, it was assumed that C, H, O were the major organic components of these samples. Other elements present in the reference materials' sheet with concentrations greater than 1% were also included. Second, to determine area density, each shrimp was weighed before being mounted and the approximate area calculated using a thresholding script in MATLAB® R2015a v8.5.0 on the Compton intensity image obtained from the μXRF map. Specifically, the Compton image of each shrimp was imported into MATLAB® and a histogram of the Compton intensities obtained. Each histogram was used to identify an intensity threshold that differentiated the Kapton® tape background from the pixels overlapping the shrimp. Pixels in the histogram above this threshold were then counted and multiplied by the pixel pitch (0.02 x 0.02 mm) to compute the total area. The shrimp mass was divided by the computed area to estimate the area density required for fluorescence yield calculations.

Analysis for Total As content by Dynamic Reaction Cell - ICP-MS

Dried baby shrimp and CRMs were analyzed for total As content by ICP-MS following acid digestion. Samples were pre-digested at ambient temperature overnight with 3 mL concentrated HNO_3. Digestion was completed using microwave-assisted heating (Discover SPD; CEM, Matthews, NC) with a maximum pressure of 375 psi (2.59 MPa). After digested samples had cooled to ambient temperature, they were diluted to 10 mL with doubly-deionized (DDI) water (18.2 MΩ cm, APS Water Services, Lake Balboa, California). Digested shrimp samples and CRMs were further diluted 1+24 with a reagent containing 0.005% (V/V) Triton-X100, 2% (V/V) HNO_3 and a Ga as the internal standard, and analyzed for total As using a PE ELAN DRC II ICP-MS (PerkinElmer, Shelton, CT) operated in Dynamic Reaction Cell (DRC) mode with 10% (V/V) H_2 in Ar to eliminate the $^{40}Ar^{35}Cl$ polyatomic interference. Instrumental details are given in Table 1. The method limit of detection was estimated at 0.12 μg/g. Method validation for total As was confirmed using the following CRMs: IRMM BCR-627; NRC DORM 2; NRC TORT 2; and NRC TORT 3 - Lobster Hepatopancreas (National Research Council, Ontario, Canada) and New York State Caprine Liver Reference Materials, G99-3 and G99-14 (New York State Dept. of Health; Wadsworth Center, Albany, NY).

Analysis for As species by LC-ICP-MS/MS

Arsenic speciation analysis was performed by coupling an Agilent 1260 Infinity series bio-inert Liquid Chromatography (LC) system to an Agilent model 8800 tandem ("Triple Quad") ICP-MS/MS instrument equipped with an Octopole Reaction Cell (ORS) to remove polyatomic interferences (Agilent Technologies, Santa Clara, CA, USA). The ICP-MS/MS was operated with O_2 in MS/MS mode with the first quadrupole (Q1) set to m/z 75 and the second quadrupole (Q2) set to m/z 91. This "mass-shift" approach can also be used to avoid the $^{40}Ar^{35}Cl$ polyatomic interference on As. A Hamilton (Reno, Nevada, USA) PRP-X 100 anion exchange column (5-µm particle size and 150 x 4.6 mm column length and diameter) was used for the stationary phase. A 0.5-µm in-line filter (IDEX Health and Science, Middleboro, MA, USA) was used to extend column life-time.

As species were separated in less than 10 minutes at ambient conditions using a modified version of a published method[37] based on isocratic elution with 2.5 mM succinic acid in 3% (v/v) HPLC grade methanol (MeOH) buffer at pH 5.6 (Sigma-Aldrich St. Louis, Missouri, USA) and at a flow rate of 1.0 mL min^{-1}. The LC eluent was filtered through a 0.2-µm Nylon membrane filter (Whatman, GE Health Care Life Sciences, Pittsburgh, PA), and pH was adjusted with distilled NH_4OH (GFS Chemicals, Columbus, OH) diluted to 10% (v/v). A Hanna 212 pH meter was used to measure pH and calibrated using Hanna pH 4.01 & 7.01 buffers (Hanna Instruments, Woonsocket, RI, USA). All standard solutions and eluents were prepared using purified DDI.

Extraction of arsenic species from CRMs and dried baby shrimp

Approximately 0.45 g of dried baby shrimp were carefully homogenized using a marble mortar and pestle, and a known mass transferred into a tared 50-mL conical polypropylene tube (Sarstedt, Newton, NC, USA). Similar masses of each CRM: BCR 627, NRC DORM-2, and NRC DORM-4 were also transferred into 50-mL conical polypropylene tubes, and 10 mL H_2O:MeOH mixture 50:50 (v/v) added to CRMs and samples. Empty tubes served as extraction blanks. All tubes were lightly capped to prevent pressurization

and placed on a hot block (PerkinElmer SPB 50-48, Waltham, MA, USA). Samples and CRMs were heated at 90 °c for 2.5 hours to achieve species extraction. Samples were cooled and centrifuged for 30 minutes at 3220 *g*. The extract supernatant was transferred into a 12-mL Monoject Syringe with Luer Lock Tip (Medtronic, Dublin, Ireland), and filtered through a 0.2-µm Whatman Nylon membrane with polypropylene housing (Whatman Inc. Florham Park, NJ, USA). Extracted samples were stored at 4°C in 15-mL polypropylene conical tubes (Falcon, Tewksburt, MA, USA) until speciation analysis was performed. Samples, standards, blanks, and CRMs were each diluted 1+9 in 1-mL polypropylene HPLC Snap Cap Vials (Agilent Technologies, Santa Clara, CA, USA). For analysis, 100 µL of samples, standards, blanks, and CRMs were diluted with 650 µL of mobile phase (2.5 mM succinic acid); 250 µL of H_2O_2 (Sigma-Aldrich St. Louis, Missouri, USA) to oxidize As(III) to As(V), thus simplifying the analysis to yield one peak for inorganic As (iAs).

Results and discussion

Portable XRF field data

The performance of the portable XRF analyzer was previously described based on data from a number of CRMs including NIST SRM 2976 Mussel Tissue and NRC TORT-2 Lobster Hepatopancreas [28]. These particular CRMs were selected for this study due to their light biological matrix and similarity to the shrimp samples. Validation data comparing the portable XRF performance with SR-µXRF are provided in Table 2. XRF combined standard uncertainties (u_c) were calculated using the standard deviation (SD) of repeated measurements and included the maximum uncertainty as reported by the software (u_{FP}), which is also called the statistical error of the reading (Equation 1):

$$u_c = \sqrt{SD^2 + (u_{FP})^2} \qquad \text{Equation 1}$$

Each CRM was analyzed in triplicate over 5 days.

With few exceptions, results for NIST 2976 Mussel Tissue by the portable XRF are in reasonable agreement (within ±20%) with the certified values, including those for As, which is the focus of this study. For those elements in SRM 2976 that are close to the limit of detection (LOD) by XRF, performance was still judged reasonable. Results for NRC TORT-2 (Table 2) also show reasonable performance for many trace elements including for As. Instrument performance at the three homes was assessed by analyzing reference material - IAEA Algae-413 for 12 elements (Fig. 2) in each of the three homes before and after the study samples (n=6), to monitor drift. A boric acid blank was also measured, and blank data confirmed all 12 elements were <1 µg/g. The data indicate a positive within-run drift for most elements that, with the exception of Mn and K, was small enough (<10%) to ignore. For Mn a 21% drift was observed in one home visit, while for K the maximum drift was 18%. A systematic positive bias (the difference between the found and true value) was observed for Hg that ranged from 10 to 17 %, while for As measurements the biases and/or drifts were less than 10%, relative to the reference values.

Samples of dried baby shrimp were analyzed on the portable XRF with a single measurement during each home visit. Results for 12 elements in dried baby shrimp are shown in Table 3 for each of the three homes visited. XRF results show some differences in the elemental composition of the shrimp samples. Only the home-prepared baby shrimp from Home A had detectable amounts of Se and Fe. The As content of the three baby shrimp samples tested varied from 30 µg/g (Home A), to 17 µg/g (Home B) to 6 µg/g (Home C).

SR-µXRF analysis

a) Preliminary studies

An exploratory study was conducted at CHESS to assess the feasibility of analyzing these shrimp samples using SR-µXRF. In particular, we evaluated the suitability of using the µXRF set-up and Maia detector at the F3 station to map the elemental distribution over the large area of one shrimp. With a total scan time of ~7h and an excitation energy of 20 keV, an elemental image of the dried baby shrimp sample from Home A was obtained, which showed the relative distribution of As, Ca and Br (Fig. 3). While quantification was not attempted for this initial study, the result showed the capabilities of this technique

that couples high-spatial resolution with the fast acquisition Maia detector. Fig. 3 clearly shows the accumulation of As (blue) in the abdominal region and thorax, with Ca (red) concentrated in the exoskeleton, and Br (green) in the pereopods and antennae.

b) Multi-elemental mapping of As, Ca, Br, and Cu in Dried baby Shrimp

Based on the results of the exploratory study, the experimental set up was optimized further for the excitation of As Kα and Kβ lines, by lowering the excitation energy to 16.15 keV, and changing the excitation monochromator from Si (111) to Si (220) to allow better energy resolution for future μXANES studies. Samples of dried baby shrimp from each of the three homes were analyzed using the optimized μXRF set-up at the F3 station and elemental distribution maps obtained (Fig. 4). The elemental maps in Figure 4 show As accumulates in two principal regions: the abdomen and the thorax/hepatopancreas. A similar distribution was observed for As in the shrimp sample from Home C, albeit at much lower levels; however, when overlaid with Ca and Br, the As is obscured. Therefore, Figure 4c shows Cu accumulation instead of As.

As evident in Fig. 4, Ca appears predominantly in the shrimp exoskeleton. [26, 38] The chemical composition of the shrimp exoskeleton has been investigated by others, and high levels of Ca along with other minerals have been found in the dried head and shell of shrimp. In fact, there has been some interest in utilizing shrimp waste due to its nutritional value.[39] It is notable that the baby dried shrimp from Home C is not as intact as A and B, as can be seen by the pieces of exoskeleton around the body of the shrimp. The shrimp exoskeleton is very fragile[26] and when dry, it can easily shatter, or fragment as seen in Fig 4c. Strontium, which is not shown in Fig. 4, followed the same distribution pattern as Ca, which is in agreement with other studies that have also reported high levels of Sr in the exoskeleton. [40, 41] Bromine occurs in relatively high concentrations in seawater and is known to be present in seafood, such that when it is detected in human bones, it is probably linked to a marine diet [42]. In other studies of the elemental composition of shrimp, a number of trace elements were detected in shrimp[38, 40, 43] but Br was not reported. In this study, Br was detected in all three shrimp samples. In Fig 4, Br is clearly concentrated in the pleopods, pereopods and in the antennae. Detecting localized accumulation of Br in these shrimp samples was only possible because of the high spatial resolution of the Maia detector

coupled with SR-μXRF. It is also possible that the Br detected in these samples could have resulted from brominated disinfectants used in shrimp farming. [44]

Copper has also been reported to accumulate in shrimp.[40, 45] Apart from some small random hot spots, Cu appears to have a relatively constant distribution in these dried baby shrimp. However, for the shrimp sample collected from Home C, distinct Cu hot spots were detected within each of the eyes (Figure 4c). These Cu hot spots were not observed for the other shrimp samples and, to the best of our knowledge, has not been reported previously. However, the accumulation of Hg in fish eyes has been reported and used for environmental risk assessment. [46]

c) Quantification of As in localized regions of interest within dried baby shrimp

Validation of quantitative measurements of As obtained by SR-μXRF and calculated using GeoPIXE™ was carried out by analyzing two biological reference materials with certified values for As. NIST SRM 2976 Mussel Tissue and NRC TORT-2 Lobster Hepatopancreas were prepared as pressed pellets (6 mm diameter; ~3 mm thickness) and mounted between two layers of 0.0025'' Kapton® tape. Table 2 shows the found values for As (in μg/g), and eight other elements by SR-μXRF and the values found by the portable XRF analyzer. Values reported in Table 2 for S, Cl, K and Ca are given in mg/g, while all others are in μg/g. The analytical performance for the portable XRF is good, and certainly more accurate than the data obtained using GeoPIXE™. The negative bias observed for the SR-μXRF data using GeoPIXE™, especially for the lighter elements, is likely due to absorption in the 0.0025'' Kapton® tape, suggesting that a thinner tape might be preferable in future studies. Yet, the GeoPIXE™ software still provides reasonable data for As in SRM 2976 Mussel Tissue and TORT-2 Lobster Hepatopancreas that are within the statistical uncertainties. It was noted that, while Cd was detected in TORT-2 using the portable XRF instrument (23 μg/g), it was not detected by SR-μXRF. This was unsurprising given the significant overlap between the Cd-L and potassium K-lines. In the SR-μXRF study, we chose to optimize the incident beam energy for detecting As, at the expense of detecting Cd. For quantification purposes, it is possible to direct GeoPIXE to select "discrete areas" or regions of interest (ROIs) of arbitrary diameter. Note that for accurate quantification, areas where no sample is present should not be included in the ROI.

Table 4 provides values for As content (in µg/g) measured in four different ROIs (1, 2, 3, 4). The four ROIs were at approximately the same location for each of the shrimp samples: ROI #1 abdominal segment (tergum); ROI #2 abdominal segment (pleuron); ROI #3 abdominal segment (6^{th}); and ROI #4 head (cephalothorax/carapace). Figure 5a depicts the location of the ROIs in which the spot diameter was varied from 0.1 to 1 mm. Varying the spot diameter changed the area of As quantification for the shrimp sample collected from Home A with the results shown in Table 4. The change in As content, between diameters, within ROI #2 was as little as 7%, however the change between diameters within ROI #4, was as much as 52%. This underscores the heterogeneity of As distribution at the sub-mm scale. Since the portable XRF has a 1-mm x-ray spot size, a 1-mm region diameter was selected in GeoPIXE™ for quantifying As in the various ROIs in the remaining two shrimp samples. The results in Table 4 show that, in these three shrimp samples, the As content ranges from 6–11 µg/g in the 6^{th} abdominal segment (ROI #3), to 11–41 µg/g in the pleuron abdominal segment (ROI #1), and 8–31 µg/g in the head (ROI #4). The highest As content was found in the home-prepared shrimp collected from Home A. The lowest As content in all three samples was found in ROI #3, which represents the 6^{th} abdominal segment in shrimp, and is largely exoskeleton (see Fig. 4 and the high Ca content). Despite being from different sources, all three shrimp show a similar distribution pattern and localized accumulations of As. When averaging the As content obtained by SR-µXRF over the whole shrimp with a 1-mm region size, the values obtained are 24 ± 16 µg/g; 20 ± 8 µg/g and 9 ± 2 µg/g for home-prepared baby shrimp (Home A), Rely dried baby shrimp (Home B) and Wei Chuan baby shrimp (Home C), respectively. These data are in a reasonable agreement with the As data obtained using the portable XRF. In the latter case, several shrimp were packed inside the XRF cup for analysis, so averaging the As data over the 4 ROIs yielded an appropriate comparison. This takes into consideration the portable XRF X-ray beam penetration depth, wherein the beam not only interrogates the shrimp in direct contact with the cup window but those stacked above it.

µXANES analysis

Further investigations of the As in these shrimp samples was carried out at CHESS using µXANES analysis to identify As species. Six different As compounds, including those containing As(III) and As (V),

and one reference material, DORM-2 NRC Dogfish Muscle for Trace Metals, containing AsB, were analyzed and μXANES data are shown in Fig. 6 (a). A shrimp sample with the highest As content (Home A) was selected for μXANES and three ROIs showing localized As accumulations were analyzed. The three ROIs were tentatively identified as the cephalothorax (x1), and two (1st and 3rd) abdominal segments, which are labelled as x2 and x3 respectively in Fig 6 (b). Note the graphic in Fig 6 (b) is the same image as shown in Fig. 4 (a), except that it has been inverted on the y-axis to match the orientation of the corresponding μXANES fluorescence map images in Fig. 7.

The As K-edge XANES spectra for inorganic As species feature a peak at 11875.0 eV for As (V) and at 11871.5 eV for As(III) as shown in Fig. 6(a). For the organoarsenic species, both AsB and for AsC the peak maxima are located at 11872.5 eV; in contrast, the methylated As species show peak maxima at 11873.5 eV for DMA and 11874.0 eV for MMA. These As K-edge data are consistent with values reported elsewhere for these arsenic compounds (i.e., within 0.1 eV).[47] The certified reference material DORM-2 also shows a peak maximum at 11872.5 eV, consistent with AsB and the CRM certificate that states most of the As is present as AsB (16.4 ± 1.1 μg/g) with the total As content of 18.0 ± 1.1 μg/g. The XANES spectrum for DORM-2 was acquired using the same dwell time as the As compounds (5 ms), however, because of the lower As content, a longer dwell time might have reduced spectral noise. An increased dwell time of 40 ms was adopted for generating XANES maps for the shrimp. XANES spectra obtained for 2 areas of the shrimp had similar white line energies and XANES spectral characteristics that were consistent with either AsB and/or AsC, with peak maxima at 11872.5 eV. To distinguish between As species having similar XANES spectra would require further work using Extended X-ray Absorption Fine Structure (EXAFS). The XANES data obtained here indicate that the As present in these shrimp is consistent with the relatively non-toxic organoarsenic species that was detected throughout the different ROIs mapped. However, definitive data on the relative distribution of AsB to AsC in these samples requires further analysis by LC-ICP-MS as described below.

The fast count rate of the Maia detector at CHESS was used to obtain a sequence of relatively smaller (few-mm-squared) μXRF maps at different incident beam energies stepping through the As μXANES edge. This process effectively creates an XRF-mode μXANES image stack for As in a matter of hours.

With this approach, it is possible to observe the spatial distribution of various As species in the sample, based on the shift in maximum intensity at different X-ray energies. For the shrimp sample from Home A (Fig. 6b) in particular, a rectangular area was selected for μXANES mapping (Fig. 7). Each region of the images in Fig. 7 exhibit the same dependence on incident-beam energy, showing a peak intensity at 11872.5 eV, suggesting that most or all of the arsenic in this region is associated with an organoarsenic species.

Total As measurements and As speciation

Results for total As content of the various CRMs and NYS Caprine Liver Reference Materials (RM) as measured by ICP-MS are shown in Table 5. For each of the CRMs, the values found are well within the expanded uncertainty of the expected values as stated on the various certificates or, in the case of the NYS RM, the published value.[48] This well-validated method for total As has been used for other studies,[37] and serves as useful comparison method to values obtained for total As in the dried baby shrimp using portable XRF analyzer (Table 2). As noted in Table 5, the comparison between the two methods takes into account that the analysis by ICP-MS is based on destructive analysis of multiple shrimp from the same batch and thus include biological variation. The agreement between portable XRF and ICP-MS is remarkably good given the sampling uncertainties.

Few CRMs exist that are certified for As species in seafood matrices. The three that were analyzed as part of this study are certified for AsB content. The certificate for one CRM, NRC DORM 2 (Dogfish Muscle for Trace Metals) expired in 2010. The AsB content of DORM 2 was re-analyzed using LC-ICP-MS, along with BCR 627 (Forms of arsenic in tuna fish tissue) and NRC DORM 4 (Fish protein). Results in Table 6 show good agreement between measured AsB content and the certificate value, which indicate the use of these CRMs is fit-for-purpose here. The data for AsB also provide validation for the speciation method. Results for the distribution of As species in the dried baby shrimp obtained by LC-ICP-MS are shown in Figure 8 and in Table 7. The results show that for the shrimp samples from all three homes, the majority of As (>95%) is present as AsB with trace amounts of AsC, DMA, MMA and iAs detected.

Conclusions

This investigation began as field-based survey of food and other items using a new portable XRF analyzer that utilized monochromatic excitation. Elevated levels (up to 30 μg/g) of As were detected in dried baby shrimp samples, a seafood snack that is consumed whole. This latter point prompted us to consider spatial distribution of As, and follow up studies were conducted at CHESS using SR-μXRF analysis using a high definition Maia detector. SR-μXRF using a Maia detector provides fast scanning that facilitates microscale visualization of shrimp morphological features, improving the discrimination of different elemental accumulations in the tissues. For the dried baby shrimp samples analyzed in this study, the distribution of Ca, Br, As, Cu was found to be non-uniform among the various structural features. As expected, the exoskeleton showed accumulation of Ca, while Br was concentrated in the pleopods, pereopods and the antennae. In one sample, Cu accumulations were detected in the shrimp eyes. Large heterogeneous accumulations of As were detected in the cephalothorax and in various abdominal segments. Many people consume the shrimp tail but discard the head and shell as marine waste. There has been some interest in utilizing such shrimp waste due to its nutritional value.[39] Our study contributes useful information on the chemical composition of these particular shrimp species by providing data on regional elemental content. In addition to providing spatial information, SR-μXRF provided estimates of As content in reasonable agreement with values obtained by both portable XRF and ICP-MS. At CHESS, μXANES was also used to characterize the As content. Results suggest As in these shrimp samples is consistent with the organoarsenic species AsB and/or AsC. A more selective and sensitive speciation method based on LC coupled to ICP-MS/MS found the majority of As (95%) is present as the largely non-toxic AsB species with traces of AsC, DMA, MMA and iAs detected. While these data confirm what might be expected for seafood such as shrimp, they confirm that speciation analysis conducted using one approach i.e., μXANES, can be confirmed and validated using another technique based on a different analytical method.

Acknowledgements

This study was supported in part by grant number R01 ES020371 from the National Institute of Environmental Health Sciences (NIEHS) to the Wadsworth Center. The contents are solely the responsibility of the authors and do not necessarily represent the views of the NIEHS or the NIH. Use of trade names is for identification purposes only and does not imply an endorsement by the New York State Department of Health or the NIH. This work is based upon research conducted at the Cornell High Energy Synchrotron Source (CHESS), which is supported by the National Science Foundation under award DMR-1332208. The authors are grateful to the CHESS staff for many helpful discussions, especially Peter Ko for suggestions regarding the XANES analysis of As standards.

References

1. FAO, *State of the World Fisheries and Aquaculture*, Fisheries and Aquaculture Department, Rome, 2014.
2. A. Cascorbi, *Wild-caught Warmwater Shrimp (Infraorder Penaeus - the Prnaeid Shrimps)*, Monterey Bay Aquarium, 2007.
3. S. Foo, *Chinese Cuisine: The Fabulous Flavors and Innovative Recipes of North America's Finest Chinese Cook*, Houghton Mifflin Company, Boston, New York. 2002.
4. K. Albala, *Three World Cuisines: Italian, Mexican, Chinese*, AltaMira Press. 2012.
5. A. Leufroy, L. Noël, D. Beauchemin and T. Guérin, *Food Chemistry*, 2012, **135**, 623-633. DOI: 10.1016/j.foodchem.2012.03.119.
6. W. Li, C. Wei, C. Zhang, M. Van Hulle, R. Cornelis and X. Zhang, *Food and Chemical Toxicology*, 2003, **41**, 1103-1110. DOI: 10.1016/S0278-6915(03)00063-2.
7. V. Lenoble, V. Deluchat, B. Serpaud and J.-C. Bollinger, *Talanta*, 2003, **61**, 267-276. DOI: http://dx.doi.org/10.1016/S0039-9140(03)00274-1.
8. C. K. Jain and I. Ali, *Water Research*, 2000, **34**, 4304-4312. DOI: http://dx.doi.org/10.1016/S0043-1354(00)00182-2.
9. G. Caumette, I. Koch, M. Moriarty and K. J. Reimer, *Science of The Total Environment*, 2012, **432**, 243-250. DOI: http://dx.doi.org/10.1016/j.scitotenv.2012.05.050.
10. K. E. Limburg, R. Huang and D. H. Bilderback, *X-Ray Spectrometry*, 2007, **36**, 336-342. DOI: 10.1002/xrs.980.
11. S. R. Ellis, A. L. Bruinen and R. M. A. Heeren, *Analytical and Bioanalytical Chemistry*, 2014, **406**, 1275-1289. DOI: 10.1007/s00216-013-7478-9.
12. A. Taylor, M. P. Day, S. Hill, J. Marshall, M. Patriarca and M. White, *Journal of Analytical Atomic Spectrometry*, 2015, **30**, 542-579. DOI: 10.1039/C5JA90001H.
13. S. Bohic, M. Cotte, M. Salomé, B. Fayard, M. Kuehbacher, P. Cloetens, G. Martinez-Criado, R. Tucoulou and J. Susini, *Journal of Structural Biology*, 2012, **177**, 248-258. DOI: http://dx.doi.org/10.1016/j.jsb.2011.12.006.
14. R. Ortega, *Nucl. Instrum. Methods Phys. Res., Sect. B*, 2005, **231**, 218-223. DOI: 10.1016/j.nimb.2005.01.060.
15. K. A. Dyl, J. S. Cleverley, P. A. Bland, C. G. Ryan, L. A. Fisher and R. M. Hough, *Geochimica et Cosmochimica Acta*, 2014, **134**, 100-119. DOI: http://dx.doi.org/10.1016/j.gca.2014.02.020.
16. J. S. Becker, A. Matusch and B. Wu, *Analytica Chimica Acta*, 2014, **835**, 1-18. DOI: http://dx.doi.org/10.1016/j.aca.2014.04.048.
17. T. Leonardo, E. Farhi, A. M. Boisson, J. Vial, P. Cloetens, S. Bohic and C. Rivasseau, *Metallomics*, 2014, **6**, 316-329. DOI: 10.1039/c3mt00281k.
18. Y. Du, P. M. Kopittke, B. N. Noller, S. A. James, H. H. Harris, Z. P. Xu, P. Li, D. R. Mulligan and L. Huang, *Annals of Botany*, 2015, **115**, 41-53. DOI: 10.1093/aob/mcu212.
19. R. Kirkham, P. A. Dunn, A. J. Kuczewski, D. P. Siddons, R. Dodanwela, G. F. Moorhead, C. G. Ryan, G. De Geronimo, R. Beuttenmuller, D. Pinelli, M. Pfeffer, P. Davey, M. Jensen, D. J. Paterson, M. D. De Jonge, D. L. Howard, M. Küsel and J. McKinlay, AIP Conference Proceedings.
20. C. Larue, H. Castillo-Michel, S. Sobanska, N. Trcera, S. Sorieul, L. Cécillon, L. Ouerdane, S. Legros and G. Sarret, *Journal of Hazardous Materials*, 2014, **273**, 17-26. DOI: http://dx.doi.org/10.1016/j.jhazmat.2014.03.014.
21. M. R. Carvalho, A. Woll and K. J. Niklas, *Journal of Experimental Botany*, 2016, **67**, 2777-2786.
22. M. S. Ramos, H. Khodja, V. Mary and S. Thomine, *Frontiers in Plant Science*, 2013, **4**. DOI: 10.3389/fpls.2013.00168.
23. O. Hachmoller, A. G. Buzanich, M. Aichler, M. Radtke, D. Dietrich, K. Schwamborn, L. Lutz, M. Werner, M. Sperling, A. Walch and U. Karst, *Metallomics*, 2016, **8**, 648-653. DOI: 10.1039/C6MT00001K.
24. N. C. Oliveira, J. H. Silva, O. A. Barros, A. P. Pinheiro, W. Santana, A. A. F. Saraiva, O. P. Ferreira, P. T. C. Freire and A. J. Paula, *Analytical Chemistry*, 2015, **87**, 10088-10095. DOI: 10.1021/acs.analchem.5b02815.

25. P. Gueriau, C. Mocuta, D. B. Dutheil, S. X. Cohen, D. Thiaudière, S. Charbonnier, G. Clément, L. Bertrand, N. E. Jalil, A. Tourani, F. Khaldoune, P. M. Brito, B. Khalloufi and H. Bourget, *PLoS ONE*, 2014, **9**. DOI: 10.1371/journal.pone.0086946.
26. M. Tadayon, S. Amini, A. Masic and A. Miserez, *Advanced Functional Materials*, 2015, **25**, 6437-6447. DOI: 10.1002/adfm.201502987.
27. A. H. Khan, S. A. Tarafdar, M. Ali, S. K. Biswas, S. Akhter, D. K. Saha, A. Islam, M. Billah, D. A. Hadi and F. B. A. Maroof, *Journal of Radioanalytical and Nuclear Chemistry-Articles*, 1989, **134**, 367-381. DOI: 10.1007/bf02278274.
28. D. Guimarães, M. L. Praamsma and P. J. Parsons, *Spectrochimica Acta Part B: Atomic Spectroscopy*, 2016, **122**, 192-202. DOI: http://dx.doi.org/10.1016/j.sab.2016.03.010.
29. Z. Chen and W. M. Gibson, *Powder Diffraction*, 2002, **17**, 99-103.
30. R. Van Grieken and A. Markowicz, *Handbook of X-ray Spectrometry: Methods and Techniques*, Marcel Dekker, New York. 1992.
31. R. Huang and D. H. Bilderback, *Journal of Synchrotron Radiation*, 2006, **13**, 74-84. DOI: 10.1107/S0909049505038562.
32. R. Huang, T. Szebenyi, M. Pfeifer, A. Woll, D. M. Smilgies, K. Finkelstein, D. Dale, Y. Wang, J. J Vila-Comamala, R. Gillilan, M. Cook and D. H. Bilderback, *Journal of Physics: Conference Series*, 2014, **493**. DOI: 10.1088/1742-6596/493/1/012034.
33. C. G. Ryan, D. P. Siddons, R. Kirkham, Z. Y. Li, M. D. De Jonge, D. J. Paterson, A. Kuczewski, D. L. Howard, P. A. Dunn, G. Falkenberg, U. Boesenberg, G. De Geronimo, L. A. Fisher, A. Halfpenny, M. J. Lintern, E. Lombi, K. A. Dyl, M. Jensen, G. F. Moorhead, J. S. Cleverley, R. M. Hough, B. Godel, S. J. Barnes, S. A. James, K. M. Spiers, M. Alfeld, G. Wellenreuther, Z. Vukmanovic and S. Borg, *Journal of Physics: Conference Series*, 2014, **499**. DOI: 10.1088/1742-6596/499/1/012002.
34. E. Lombi, M. D. de Jonge, E. Donner, P. M. Kopittke, D. L. Howard, R. Kirkham, C. G. Ryan and D. Paterson, *PLoS ONE*, 2011, **6**, e20626. DOI: 10.1371/journal.pone.0020626.
35. C. G. Ryan and D. N. Jamieson, *Nuclear Instruments and Methods in Physics Research Section B: Beam Interactions with Materials and Atoms*, 1993, **77**, 203-214. DOI: http://dx.doi.org/10.1016/0168-583X(93)95545-G.
36. C. G. Ryan, J. S. Laird, L. A. Fisher, R. Kirkham and G. F. Moorhead, *Nuclear Instruments and Methods in Physics Research Section B: Beam Interactions with Materials and Atoms*, 2015, **363**, 42-47. DOI: http://dx.doi.org/10.1016/j.nimb.2015.08.021.
37. G. Raber, N. Stock, P. Hanel, M. Murko, J. Navratilova and K. A. Francesconi, *Food Chemistry*, 2012, **134**, 524-532. DOI: https://doi.org/10.1016/j.foodchem.2012.02.113.
38. K. Jung and G. P. Zauke, *Aquatic Toxicology*, 2008, **88**, 243-249. DOI: http://dx.doi.org/10.1016/j.aquatox.2008.05.007.
39. H. M. Ibrahim, M. F. Salama and H. A. El-Banna, *Food / Nahrung*, 1999, **43**, 418-423. DOI: doi:10.1002/(SICI)1521-3803(19991201)43:6<418::AID-FOOD418>3.0.CO;2-6.
40. N. P. C. Tu, N. N. Ha, T. Ikemoto, B. C. Tuyen, S. Tanabe and I. Takeuchi, *Marine Pollution Bulletin*, 2008, **57**, 858-866. DOI: http://dx.doi.org/10.1016/j.marpolbul.2008.02.016.
41. A. C. Brannon and K. R. Rao, *Comparative Biochemistry and Physiology Part A: Physiology*, 1979, **63**, 261-274. DOI: http://dx.doi.org/10.1016/0300-9629(79)90158-0.
42. D. Guimarães, A. A. Dias, M. Carvalho, M. Carvalho, J. Santos, F. Henriques, F. Curate and S. Pessanha, *Quantitative Determinations and Imaging in Different Structures of Buried Human Bones*. 2016.
43. E. Silva, Z. C. V. Viana, C. R. E. Onofre, M. G. A. Korn and V. L. C. S. Santos, *Brazilian Journal of Biology*, 2016, **76**, 194-204.
44. S. Gräslund and B.-E. Bengtsson, *Science of The Total Environment*, 2001, **280**, 93-131. DOI: http://dx.doi.org/10.1016/S0048-9697(01)00818-X.
45. M. S. Hossain and Y. S. A. Khan, *Sci Asia*, 2001, **27**, 165-168.
46. P. Pereira, J. Raimundo, O. Araújo, J. Canário, A. Almeida and M. Pacheco, *Science of The Total Environment*, 2014, **494**, 290-298. DOI: http://dx.doi.org/10.1016/j.scitotenv.2014.07.008.
47. P. G. Smith, I. Koch, R. A. Gordon, D. F. Mandoli, B. D. Chapman and K. J. Reimer, *Environmental Science & Technology*, 2005, **39**, 248-254. DOI: 10.1021/es049358b.
48. P. C. Kruger, C. Geraghty and P. J. Parsons, *Accreditation and Quality Assurance: Journal for Quality, Comparability and Reliability in Chemical Measurement*, 2010, **15**, 451-458.

Figure 1. Sample preparation for SR-μXRF analysis at the CHESS F3 station: (a) shrimp and CRM pellet mounted on 24x36 mm slide using Kapton® tape and (b) a powdered As compound contained within a teflon washer and secured with Kapton® tape.

a)

b)

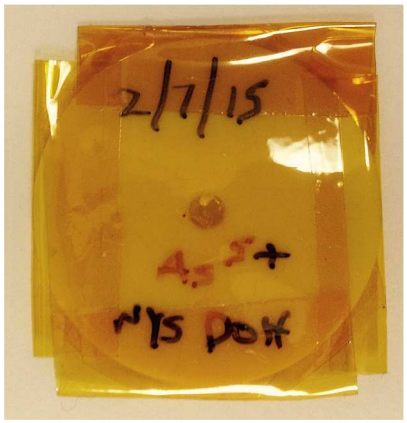

Figure 2. Portable XRF performance across three homes monitored for 12 elements using RM IAEA Algae-413. Data for the beginning (full circles) and the end (open circles) of each run are shown by home. Elements are grouped as follows: (a) Cd, Mn, Ni, Hg and Cu; (b) Cr, Pb, Zn, As; (c) K, Ca and Fe.

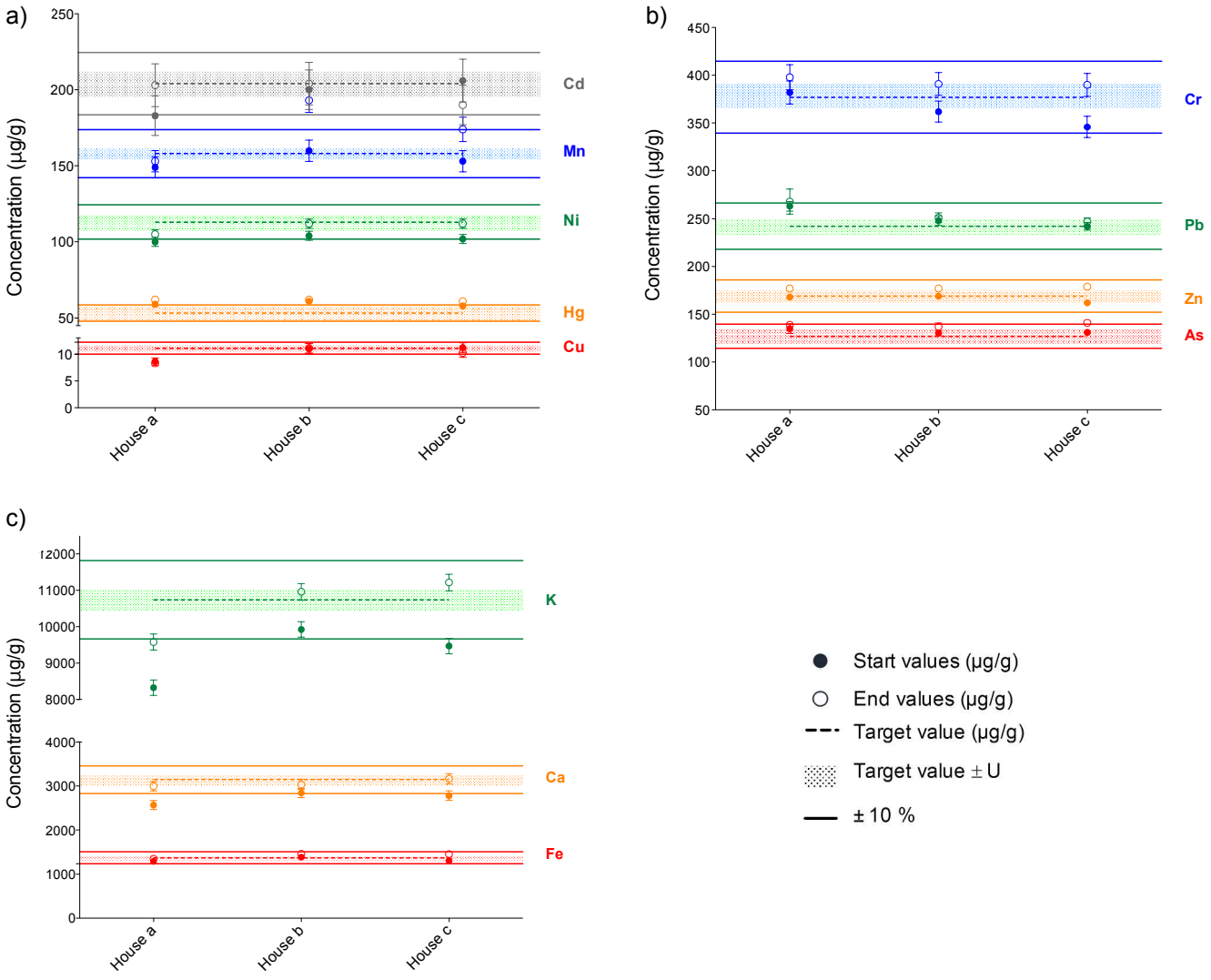

Figure 3. Elemental image (12 x 20 mm) of a dried baby shrimp obtained by SR-μXRF with a MAIA detector. The data were acquired on the F3 beamline at CHESS using a shrimp sample collected at home A. The three-element RGB image shows As (blue), Ca (red) and Br (green).

Figure 4. Elemental images of dried baby shrimp samples using SR-μXRF with a Maia detector. Three element RGB images show shrimp samples collected from (a) Home A, As (blue), Ca (red) and Br (green), 13 x 17 mm; b) Home B, As (blue), Ca (red) and Br (green), 15 x 18 mm; and c) Home C, Cu (blue), Ca (red) and Br (green), 12 x13 mm.

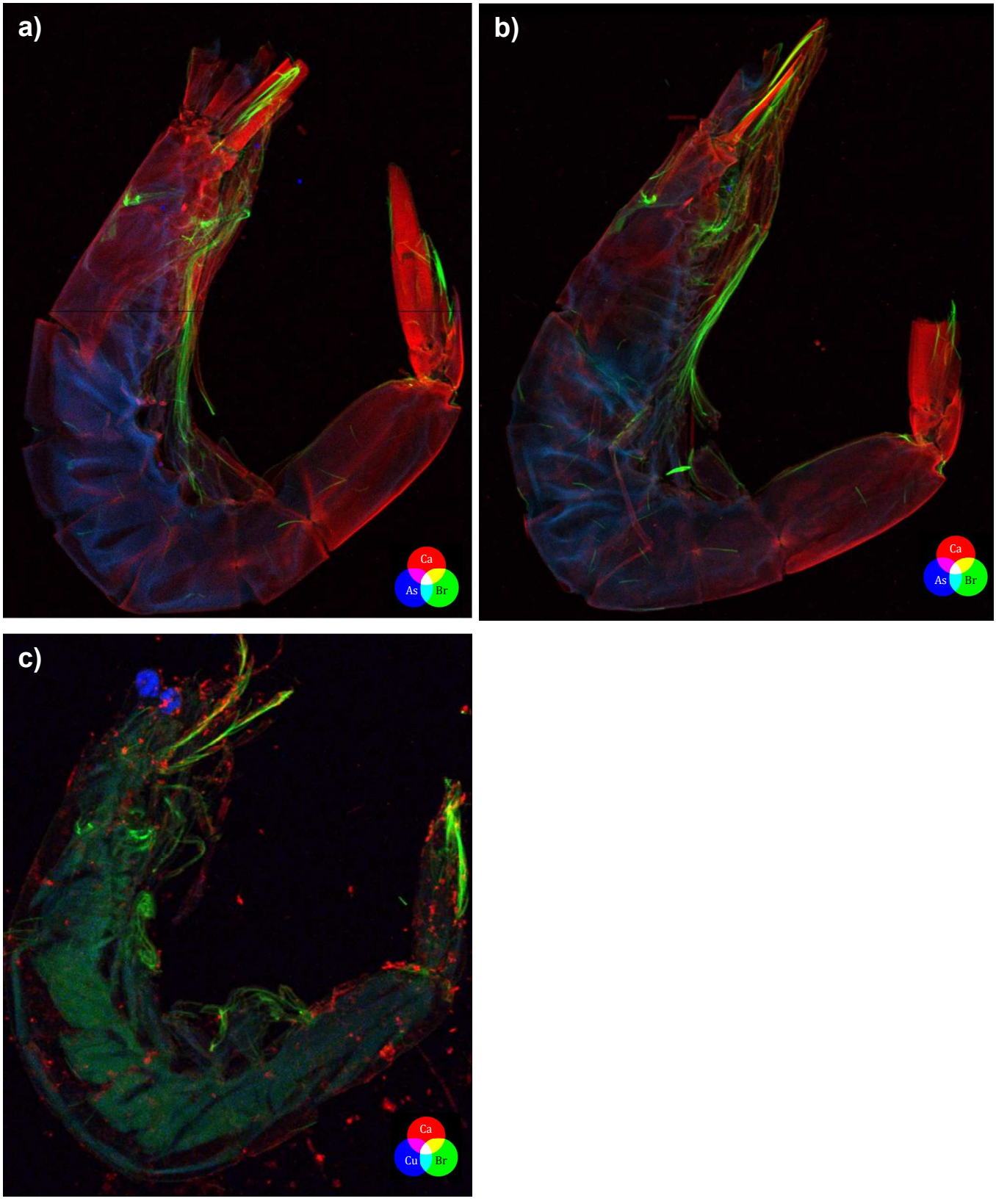

Figure 5. SR-μXRF maps obtained at CHESS showing As distribution in dried baby shrimp, with 4 ROIs denoted as 1, 2, 3 and 4. The brightest regions correspond to higher As accumulations. The shrimp sample from (a) Home A shows each of the 4 ROIs analyzed using diameters of 0.1 mm, 0.5 mm and 1 mm. The shrimp samples from (b) home B and (c) home C were analysed using a 1-mm region diameter.

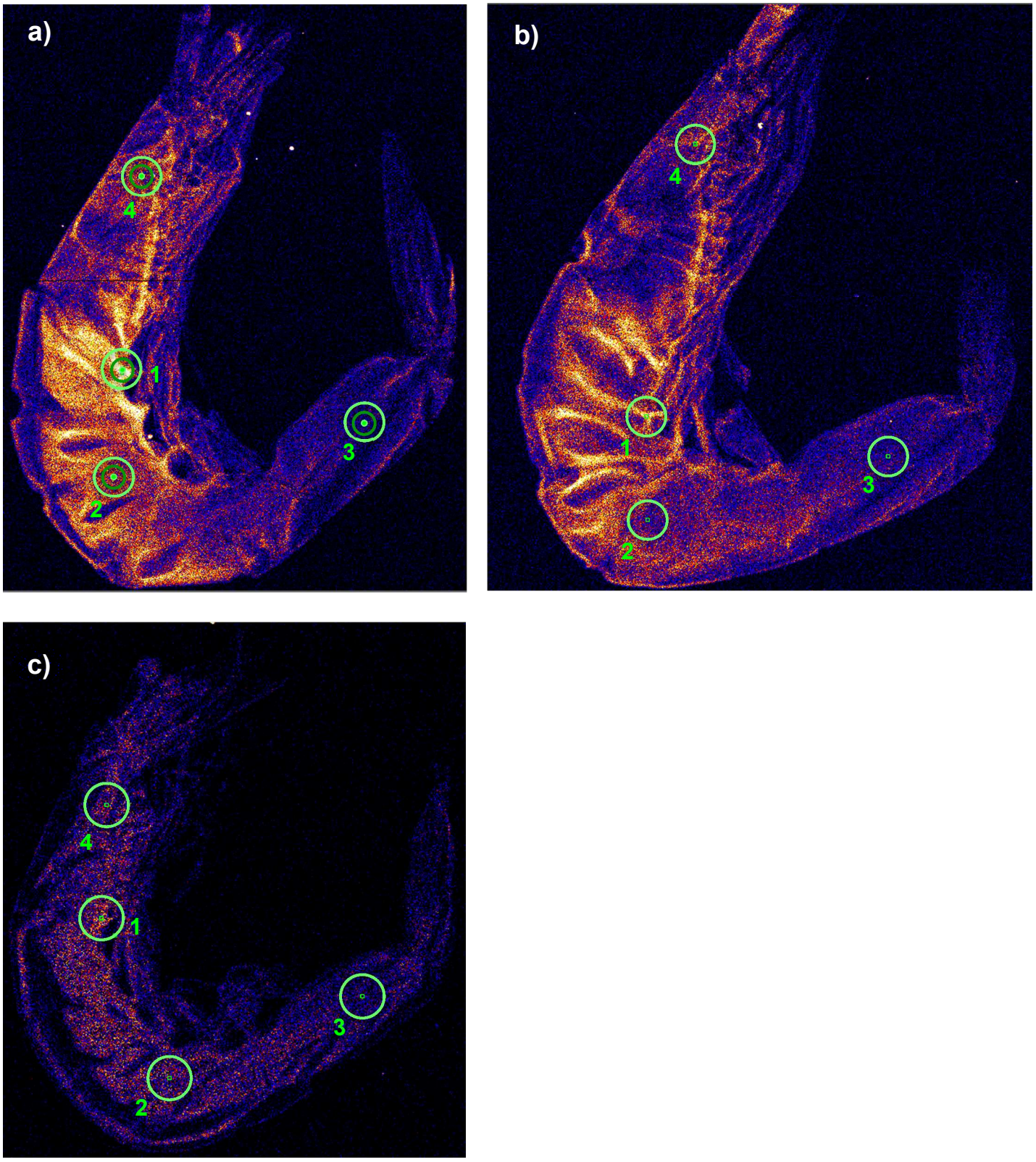

Figure 6. (a) Arsenic K-edge fluorescence μXANES spectra for various As compounds, a reference material and three ROIs in a shrimp from Home A. (b) An SR-μXRF elemental image (As, Ca, Br) of the shrimp identifies the specific ROIs analysed using μXANES. The yellow rectangle indicates the location used to obtain the μXANES map shown in Figure 7.

(a) (b)

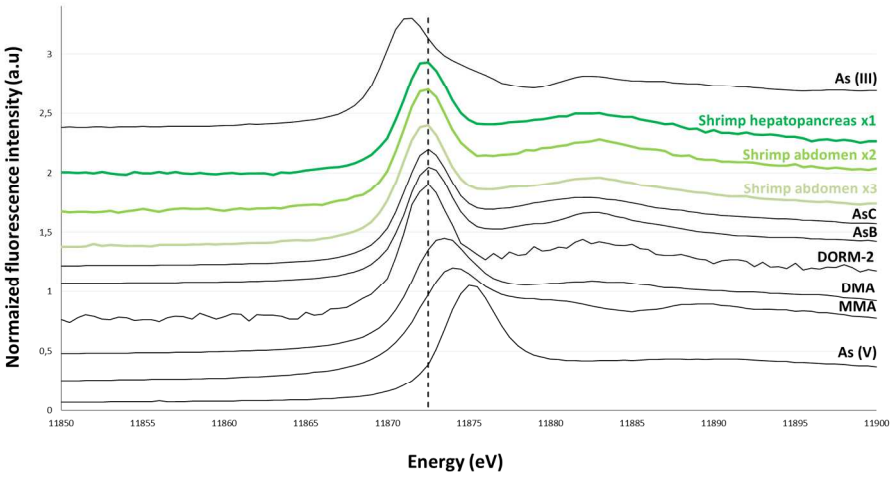

Figure 7. μXANES fluorescence maps for As K-edge, using a enriched As containing area of baby dried shrimp from home A, shown in Fig 6. X-ray energies ranged from 11850.5 eV to 11894.5 eV using a dwell time of 40 ms. White corresponds to the highest relative As content and black to the lowest.

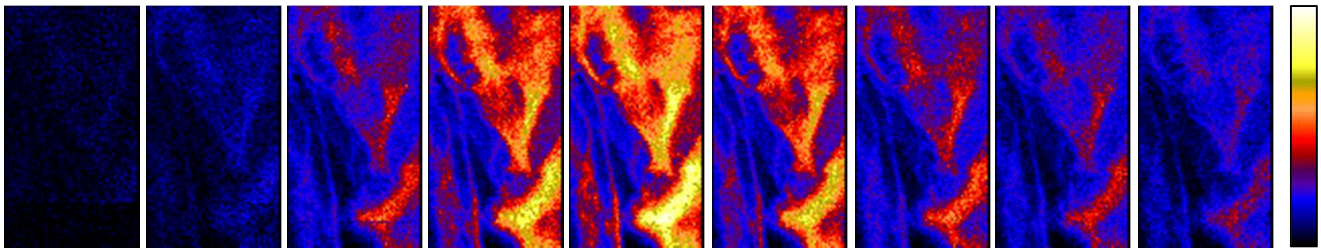

Figure 8. As speciation analysis of dried baby shrimp by LC-ICP-MS/MS: As(III) and As (V) are combined as iAs